

PAPER

## A comprehensive analysis of the CVD growth of boron nitride nanotubes

To cite this article: Amir Pakdel *et al* 2012 *Nanotechnology* **23** 215601

View the [article online](#) for updates and enhancements.

### You may also like

- [Energetics and electronic structures of single walled carbon nanotubes encapsulated in boron nitride nanotubes](#)  
Kaoru Hisama, Shohei Chiashi, Shigeo Maruyama *et al.*
- [Towards sustainable transparent flexible heaters: Integration of a BNNT interlayer using green solvent substitution](#)  
Kaitlin Wagner, Shan Zou, Yadienka Martinez-Rubi *et al.*
- [Boron nitride nanotube scaffolds: emergence of a new era in regenerative medicine](#)  
Sathyan Vivekanand Anandhan and Uma Maheswari Krishnan



**ECS**  
The  
Electrochemical  
Society  
Advancing solid state &  
electrochemical science & technology

**DISCOVER**  
how sustainability  
intersects with  
electrochemistry & solid  
state science research

# A comprehensive analysis of the CVD growth of boron nitride nanotubes

Amir Pakdel<sup>1,2</sup>, Chunyi Zhi<sup>1</sup>, Yoshio Bando<sup>1</sup>, Tomonobu Nakayama<sup>1,2</sup>  
and Dmitri Golberg<sup>1,2</sup>

<sup>1</sup> International Center for Materials Nanoarchitectonics (MANA), National Institute for Materials Science (NIMS), Namiki 1-1, Tsukuba, Ibaraki 305-0044, Japan

<sup>2</sup> Graduate School of Pure and Applied Sciences, University of Tsukuba, Tennodai 1, Tsukuba, Ibaraki 305-0005, Japan

E-mail: [PAKDEL.Amir@nims.go.jp](mailto:PAKDEL.Amir@nims.go.jp) and [GOLBERG.Dmitri@nims.go.jp](mailto:GOLBERG.Dmitri@nims.go.jp)

Received 21 February 2012, in final form 22 February 2012

Published 3 May 2012

Online at [stacks.iop.org/Nano/23/215601](http://stacks.iop.org/Nano/23/215601)

## Abstract

Boron nitride nanotube (BNNT) films were grown on silicon/silicon dioxide (Si/SiO<sub>2</sub>) substrates by a catalytic chemical vapor deposition (CVD) method in a horizontal electric furnace. The effects of growth temperature and catalyst concentration on the morphology of the films and the structure of individual BNNTs were systematically investigated. The BNNT films grown at 1200 and 1300 °C consisted of a homogeneous dispersion of separate tubes in random directions with average outer diameters of ~30 and ~60 nm, respectively. Meanwhile, the films grown at 1400 °C comprised of BNNT bundles in a flower-like morphology, which included thick tubes with average diameters of ~100 nm surrounded by very thin ones with diameters down to ~10 nm. In addition, low catalyst concentration led to the formation of BNNT films composed of entangled curly tubes, while high catalyst content resulted in very thick tubes with diameters up to ~350 nm in a semierect flower-like morphology. Extensive transmission electron microscopy (TEM) investigations revealed the diameter-dependent growth mechanisms for BNNTs; namely, thin and thick tubes with closed ends grew by base-growth and tip-growth mechanisms, respectively. However, high catalyst concentration motivated the formation of filled-with-catalyst BNNTs, which grew open-ended with a base-growth mechanism.

 Online supplementary data available from [stacks.iop.org/Nano/23/215601/mmedia](http://stacks.iop.org/Nano/23/215601/mmedia)

(Some figures may appear in colour only in the online journal)

## 1. Introduction

A boron nitride nanotube (BNNT) is a structural analog of a carbon nanotube (CNT) in which alternating boron (B) and nitrogen (N) atoms entirely substitute for carbon (C) atoms in a rolled-up graphitic-like sheet with almost no change in the atomic spacing. However, in contrast to CNTs, BNNTs are electrical insulators with a wide bandgap of ~6 eV, which is basically independent of the tube chirality and morphology [1]. This difference in the electronic structures of these nanomaterials results in distinctive luminescence emissions, i.e., after excitation by electrons or photons, BNNTs emit violet or ultraviolet

(UV) luminescence, while CNTs emit infrared light with chirality-dependent wavelength [2]. In addition, a layered BN structure is known to have notably higher thermal resistance and chemical stability compared to a graphitic C structure [3, 4]. Moreover, BNNTs have exhibited superb mechanical robustness and excellent thermal conductivity like their C counterparts [5]. Therefore, BNNTs could be of special interest for various applications such as protective shields encapsulating nanomaterials (e.g., metallic or semiconducting nanowires, nanorods, and nanoparticles, in particular those performing at high temperatures or in chemically harsh environments), nanofillers for insulating composite materials, and UV lasers [5, 6].

BNNTs can be grown by a variety of means, such as arc discharge [7], laser ablation [8], chemical vapor deposition (CVD) [9], ball milling [10], substitution reaction of CNTs [11, 12], atom deposition [13], and the plasma-jet method [14]. Obviously, finding the clues to fully optimize the production of BNNTs requires a good understanding of their growth mechanism in different formation conditions. Furthermore, since the properties of low-dimensional materials strongly depend on their structural characteristics (such as size, shape, and surface states), the controllable synthesis of one-dimensional (1D) BN nanostructures is extremely important with regard to investigations of their fundamental properties [15]. So far, few reports have focused on the growth mechanism of BN nanomaterials (usually considering only one special synthesis condition), and very rarely has there been a comprehensive study on the effect of growth conditions on the structure and formation mechanism of these nanostructures [15, 16].

Here we report a comprehensive study on the growth, structure, and morphology of 1D BN nanostructures selectively prepared under different synthesis conditions by a thermal CVD method. Different concentrations of B, magnesium oxide (MgO), and iron oxide (FeO) powders were used as precursor materials in a conventional horizontal tube furnace under an ammonia (NH<sub>3</sub>) gas flow at different temperatures to produce snow-white BN nanostructure films on silicon/silicon dioxide (Si/SiO<sub>2</sub>) substrates. An extensive electron microscopy analysis of the present 1D BN nanostructures provides us with guidelines to better understand their CVD synthesis and the mechanisms governing their growth.

## 2. Experimental details

### 2.1. CVD growth of BNNTs

The CVD growth of the crystalline BNNTs was performed in an electric horizontal tube furnace, in a setup slightly different from the ones previously reported [17, 18]. In brief, the precursor powders (B:FeO:MgO) were mechanically mixed at the molar ratios of 1:1:1, 2:1:1, and 4:1:1 and were positioned in an alumina combustion boat covered with a Si/SiO<sub>2</sub> substrate. The boat was then placed inside an alumina test tube with both ends open, and they were set into a horizontal alumina vacuum chamber. The chamber was evacuated to ~1 Torr and then ammonia gas flowed at the rate of 0.4 ml min<sup>-1</sup>. The precursors were heated to 1200, 1300, and 1400 °C, held for 30 min, and then cooled to room temperature. A photograph of the white BN products covering the substrate, precursors, and walls of the combustion boat is presented in the supplementary data, figure S1 (available at [stacks.iop.org/Nano/23/215601/mmedia](http://stacks.iop.org/Nano/23/215601/mmedia)).

### 2.2. Characterization techniques

The morphologies of the grown BNNT films were studied by a field emission scanning electron microscope (FE-SEM; Hitachi SU8000). The structure and chemical composition

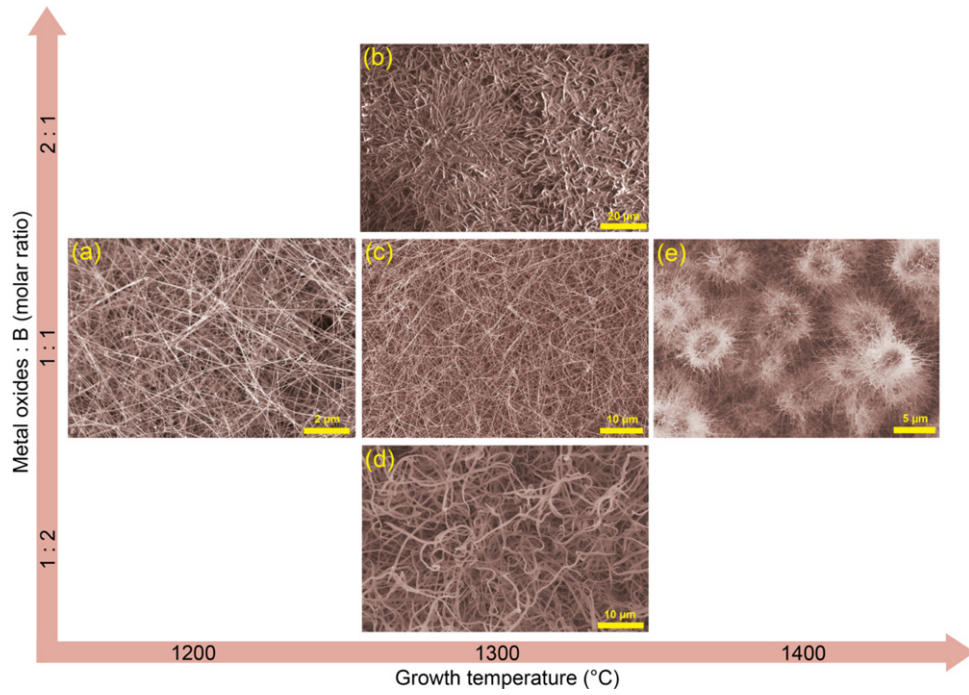
of the BNNTs were analyzed by a high-resolution field emission transmission electron microscope (HRTEM; JEOL JEM-2100F) equipped with an electron energy loss spectrometer (EELS), energy-dispersive x-ray spectrometer (EDS), and high-angle annular dark-field imaging (HAADF) scanning transmission electron microscope (STEM) accessories. Raman spectroscopy (LabRam HR-800) was also utilized at room temperature to investigate the purity of the BNNTs.

## 3. Results and discussion

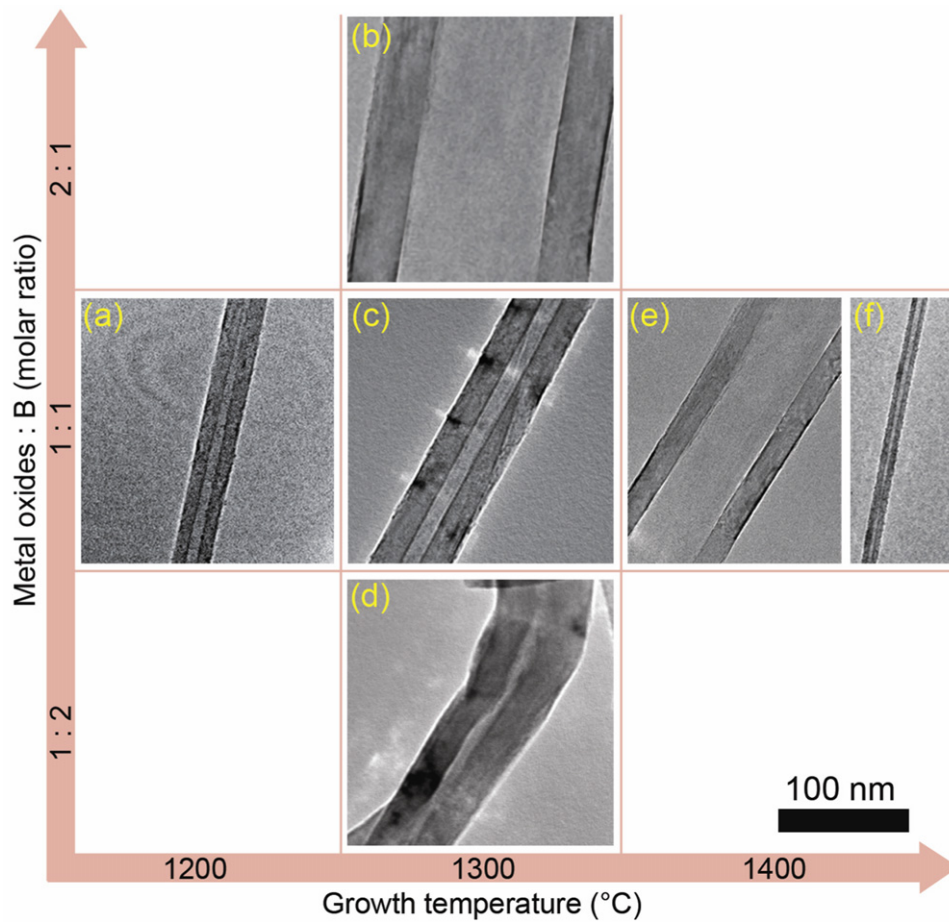
### 3.1. BNNT growth control

Figure 1 shows the low-magnification scanning electron microscope (SEM) images of the samples prepared at different growth conditions. It is noticed that the morphology of the BNNT films is strongly dependent on the process variables, i.e., molar ratios of the precursor materials and the growth temperature. The influence of growth temperature on the morphology of the BNNT films is noticeable in figures 1(a), (c), and (e), depicting the products synthesized at 1200, 1300, and 1400 °C, respectively. The films grown at 1200 and 1300 °C consist of long straight nanotubes lying on the substrate in various random directions, though a comparison of their SEM images reveals that the ones prepared at 1200 °C are thinner. The nanotubes grown at 1400 °C, on the other hand, have formed bundles on the substrate with a flower-like morphology. The effect of catalyst content on the morphology of the BNNT films is depicted in figures 1(b)–(d), keeping in mind that increasing the metal oxide concentration in the precursor materials represents an increase in the catalyst content. When the metal oxide molar ratio in the precursor materials was low, the nanotubes grew in an entangled curly fashion (figure 1(d)). On increasing the amount of metal oxide in the precursor materials, straight nanotubes with large aspect ratios were formed (figure 1(c)), and further increase of the oxide concentration led to the growth of nanotubes and nanofibers with large diameters in a randomly tilted semierect flower-like morphology (figure 1(b)).

Further characterization of the products was performed by transmission electron microscopy (TEM). Figure 2 depicts the effect of the process variables on the average diameter of the BNNTs. The effect of synthesis temperature on the average outer diameter of the nanotubes is shown in figures 2(a), (c), (e), and (f). Raising the growth temperature from 1200 to 1300 °C resulted in an increase of the tubes' average diameter from ~30 to ~60 nm. However, at 1400 °C a combination of BNNTs with both small and large diameters was obtained with average diameters of ~20 and ~100 nm, respectively. It was also noticed that the BNNT size distribution became broader by raising the synthesis temperature (supplementary data, figure S2, available at [stacks.iop.org/Nano/23/215601/mmedia](http://stacks.iop.org/Nano/23/215601/mmedia)). A comparison between figures 2(b)–(d) shows that higher metal oxide content in the precursor materials also led to an overall increase of the outer diameter of the BNNTs.



**Figure 1.** Effect of growth temperature and catalyst concentration on the morphology of BNNT films, as revealed by SEM.



**Figure 2.** Effect of growth temperature and catalyst concentration on the outer diameter of BNNTs, as revealed by TEM.

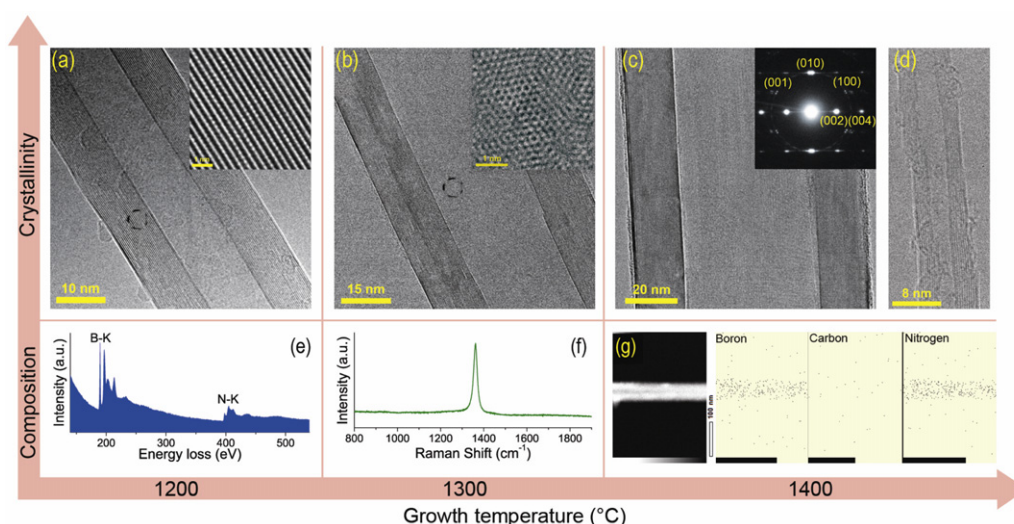


**Figure 3.** Representative HRTEM images of the BNNTs grown at (a) 1200 °C, (b) 1300 °C, and (c) and (d) 1400 °C. (e) Typical EEL spectrum of the BNNTs grown at 1200 °C. (f) Typical Raman spectrum of the BNNTs grown at 1300 °C. (g) HAADF STEM elemental maps of a typical BNNT grown at 1400 °C.

### 3.2. Effect of growth temperature

Figures 3(a), (b) and (c)–(d) show typical high-resolution TEM (HRTEM) images of the as-grown 1D nanostructures synthesized at 1200 °C, 1300 °C, and 1400 °C, respectively, consisting of parallel and straight walls. The inset of figure 3(a) is a magnified image of tubular shells grown at 1200 °C. It illustrates well-ordered fringes with an interlayer distance of 0.33–0.34 nm, which is characteristic of crystallization of h-BN (002) planes [1]. The inset of figure 3(b) is an enlarged image of the central part of the nanotube grown at 1300 °C depicting the hexagonal arrangement of atoms in the BNNT. The selected area electron diffraction (SAED) pattern from the BNNT grown at 1400 °C (inset of figure 3(c)) confirms the good crystallinity of the tube [19]. In general, each wall of a nanotube contributes to two sets of hexagonal diffraction spots in an SAED pattern, depending on the chirality of the nanotube. In the special cases of zigzag and armchair tubes, these two sets of spots will overlap and a single hexagonal set of diffraction spots will be observed. Unlike multi-walled CNTs, where the chirality of each layer is independent of the others, BNNTs usually show grouping of chiral angles around an average value due to their strongly correlated layers (i.e., the B atoms in one layer have to be aligned with the N atoms in the neighboring layer) [20]. The (010) reflections in the diffraction pattern come from portions of hexagonal nets which are perpendicular to the incident electron beam. The angle between the tube axis and the (010) reflection (represented by  $\theta_{101}$ ) is equal to the chiral angle (except in very thin tubes with diameters less than  $\sim 3$  nm) [21]. Therefore, BNNTs with armchair and zigzag hexagon arrangements exhibit (010) reflections at  $\theta_{101} = 30^\circ$  and  $\theta_{101} = 0^\circ$ , respectively. The present (010) reflections in the diffraction pattern indicate that the BNNT has a zigzag chirality. The majority of the BNNTs studied here showed zigzag or near zigzag chiralities with a narrow range of chiral angle distribution between 0 and  $5^\circ$ , and very rarely

did we observe reflections originating from armchair-type layers. These results are in agreement with other experimental data [22] and theoretical calculations [23], showing that the zigzag-type BN structure is energetically more favorable and thus more stable than the armchair-type structure.

In order to verify the composition of the nanotubes, we initially performed electron energy loss spectroscopy (EELS), which is particularly effective for characterizing the chemical composition of nanomaterials made of light elements (e.g., B, C, and N). Figure 3(e) shows a typical EEL spectrum of the nanotubes grown at 1200 °C, demonstrating two absorption features at  $\sim 188$  and  $\sim 401$  eV attributed to B and N K-edges, respectively. The absence of a C K-edge at  $\sim 285$  eV indicates the purity of the BNNTs. The sharp profiles of the  $\pi^*$  peaks for B and N determine the  $sp^2$ -type bonding of hexagonal BN. The quantification of the spectrum indicates a B:N composition ratio of  $\sim 1:1$  [24]. Similar features were observed in the EEL spectra of the BNNTs synthesized at 1300 and 1400 °C as well (supplementary data, figure S3, available at [stacks.iop.org/Nano/23/215601/mmedia](http://stacks.iop.org/Nano/23/215601/mmedia)). High-angle annular dark-field imaging (HAADF) scanning transmission electron microscopy (STEM) was also utilized to identify the chemical composition of the nanotubes due to its good spatial resolution and high sensitivity to variations of the atomic number of elements. The HAADF STEM elemental maps in figure 3(g) confirm the purity of a typical BNNT grown at 1400 °C and demonstrate that B and N are uniformly distributed along and across the nanotube.

The as-grown BNNTs were also characterized by Raman spectroscopy. Figure 3(f) depicts a sharp Raman peak at  $\sim 1366$   $cm^{-1}$  for the BNNTs grown at 1300 °C. The BNNTs synthesized at 1200 and 1400 °C also showed the Raman shift at  $1366$   $cm^{-1}$  (supplementary data, figure S4 available at [stacks.iop.org/Nano/23/215601/mmedia](http://stacks.iop.org/Nano/23/215601/mmedia)), which is attributed to the  $E_{2g}$  mode, i.e., the high frequency counterphase vibrational mode due to B and N atoms moving against each other within a plane [25, 26]. The present Raman results

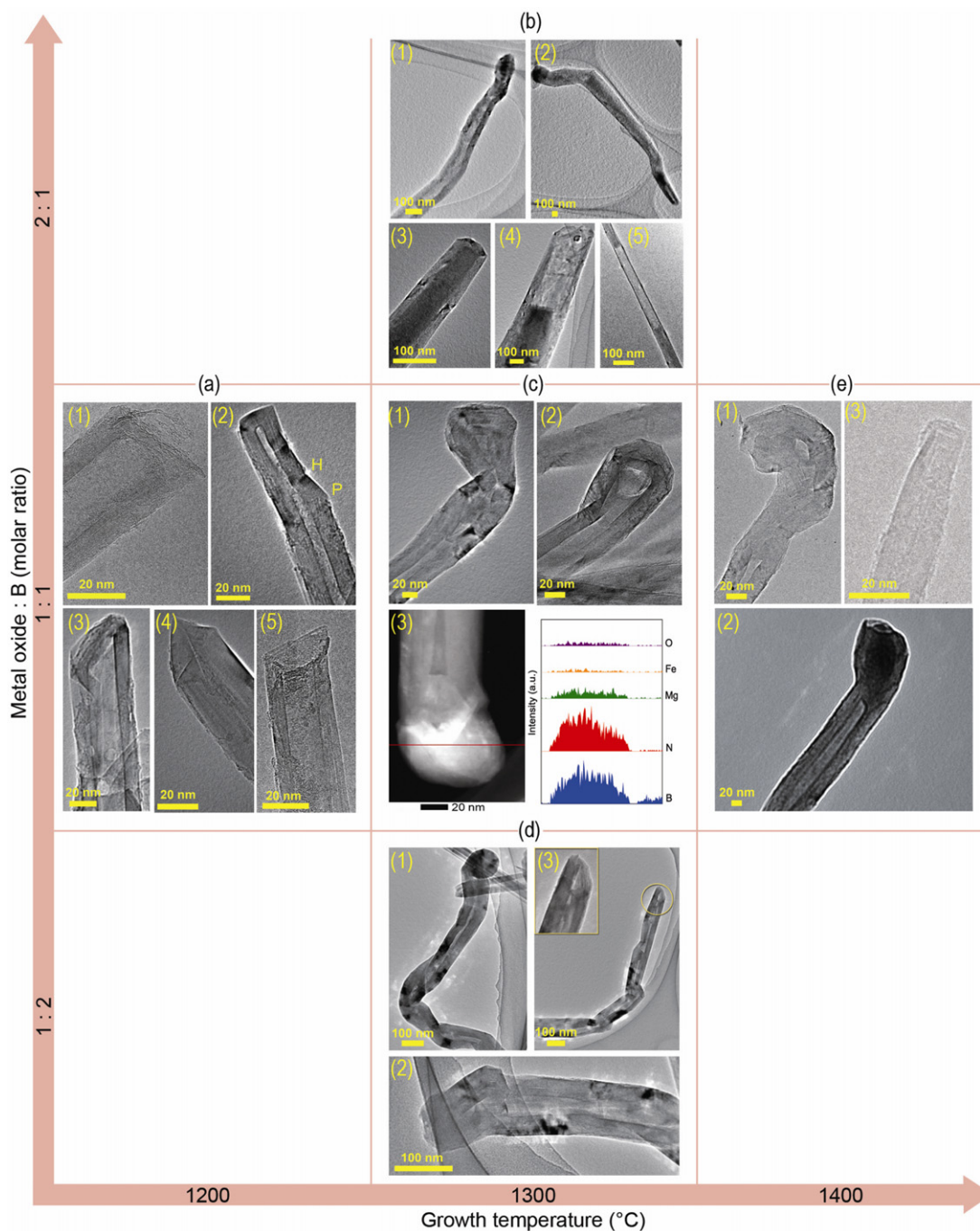


**Figure 4.** TEM analysis of the tip-ends of the BNNTs grown in different conditions.

are similar to those reported for bulk h-BN [25–29] due to the multilayer structure of the BNNTs. Although it has been calculated that a frequency shift of the tube phonon with respect to the phonon of bulk h-BN can occur due to the change of average tube diameters in thin samples ( $<3$  nm) [28], a tube diameter dependence of the Raman shift was not observed in the present BNNTs with diameters ranging between  $\sim 10$  and  $\sim 100$  nm. The Raman spectrum in figure 3(h) also proves the high purity of the present BNNTs since there is no trace of the carbon G band at  $\sim 1600$   $\text{cm}^{-1}$ .

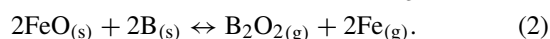
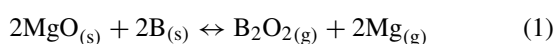
To understand the growth mechanism of the BNNTs in different conditions, a large number of tube ends were

investigated in TEM. Figure 4 illustrates a collection of various tips observed in the BNNTs. Most of the examined nanotubes, which were synthesized at an equal molar ratio of metal oxides and B, had closed ends regardless of the synthesis temperature. The majority of the BNNTs synthesized at  $1200$   $^{\circ}\text{C}$  showed characteristic flat tips consisting of fringes perpendicular to the tube axis, similar to the first-time observations of Loiseau *et al* [30] and Terrones *et al* [31]. Figure 4(a)(1) represents the most commonly observed tip morphology, i.e., a flat tip with right-angle corners which is distinguishable from CNT tip-ends. The right-angle termination results from the incorporation of four

member rings at the tip, instead of five member rings. Even member rings (e.g., squares, hexagons, and octagons) preserve B–N bonds, while odd member rings (e.g., pentagons and heptagons) introduce energetically less favorable B–B or N–N bonds [21]. Nevertheless, in special cases, such as nanotubes with bill-shaped terminations, the presence of pentagons and heptagons in the structure has been suggested [32], as indicated by ‘P’ and ‘H’ in figure 4(a)(2), respectively. The triangular flag-shaped tip shown in figure 4(a)(3) also indicates the presence of odd member rings. Similar tip-ends have been discussed by Saito *et al* [21] in BNNTs synthesized via an arc discharge method. In the present BNNTs, we seldom observed tubes with a sharp end (having a cone-like termination) or open ends as shown in figures 4(a)(4) and (5), respectively.

The tubes synthesized at higher temperatures, on the other hand, displayed other features. More open tip-ends and numerous BNNTs with complex tip shapes and encapsulated particles were observed in BNNTs grown at 1300 °C, as shown in figures 4(c)(1) and (2), respectively. These observations revealed that the BNNTs had a catalytic growth mechanism. Figure 4(c)(3) shows a typical HAADF image of a BNNT encapsulating a particle and its corresponding energy-dispersive x-ray spectra (EDS). It displays a considerable amount of Mg, a small amount of Fe, and some O at the tip-end, indicating that the main catalyst for the growth of the present BNNTs was Mg. Similar results were obtained from the analysis of several tubes, i.e., either a very small amount of Fe or none was detected at the tip-ends. For the tubes grown at 1400 °C, a diameter-related tip morphology was recognized, i.e., encapsulated particles were mainly found in tubes with diameters larger than ~30 nm; however, thinner BNNTs usually showed flat tip-ends without any trace of metallic particles, as depicted in figures 4(e)(1), (2) and (3), respectively.

During heating of the precursors, the B and catalyst oxides react to form growth vapors, according to the following equations [33]:



Boron oxide ( $\text{B}_2\text{O}_2$ ) is believed to be an effective precursor for the growth of BNNTs through the interaction with  $\text{NH}_3$  [33], as shown in the following equation:



According to the vapor–liquid–solid (VLS) mechanism [34], nanosized liquid or partially melted particles of catalysts are condensed on the substrate when their partial vapor pressures are sufficient. The BN species then diffuse into the condensed catalyst aggregates leading to supersaturation and the subsequent precipitation of BNNTs. Considering the encapsulated particles and flat tip-ends in thick and thin BNNTs, respectively, we suggest a tip-growth model for the former tubes and a base-growth model for the latter ones.

Generally it is believed that in the base-growth model the catalyst particle adherence to the substrate surface is strong enough; thus, the nanotube precipitates from the top

surface of the particle and the filament continues to grow with the particle anchored to the substrate [35]. Figure 5(a) illustrates the base-growth model for a nanotube with a closed tip-end. First, the catalyst atoms aggregate into nanosized particles, serving as the basis for the nanotube growth. Then, the reactions leading to BN species formation occur on the surface of the catalyst particle and, upon supersaturation, BN shells precipitate layer by layer. With the growth of BN layers, the strain energy at the interface between the newly formed BN shell and the particle increases, and consequently an inter-void is formed. The BNNT then lengthens with a closed end through BN feedstock supply from the base, where the nanotube interfaces with the anchored catalyst. Multi-wall formation in the present nanotubes indicates that the size of the catalyst particles was not small enough for the formation of single-wall nanotubes. We attribute the base-growth model to the BNNTs synthesized at the lowest temperature (1200 °C).

However, on increasing the synthesis temperature to 1300 °C, the tip-growth model is suggested to be the main mechanism for the growth of the BNNTs with larger diameters. In this case, a BNNT precipitates out across the catalyst bottom pushing the whole particle off the Si/SiO<sub>2</sub> substrate, as depicted in figure 5(c). As long as the particle surface is actively available for the formation and diffusion of BN species, the BNNT will grow longer. However, once the particle is fully covered with excess BN or its surface is fully oxidized, its catalytic activity and consequently the BNNT growth will stop. The tip-growth mechanism is believed to occur when the catalyst–substrate interaction is weak [35]. However, considering our experimental set up and the increase of the growth temperature, it is plausible to think that the large liquid catalysts particles had to be suspended from the substrate surface; therefore, capillarity or gravity could also be the driving force for their carriage along the growing nanotubes.

At the highest synthesis temperature (1400 °C), the catalytic metal atoms agglomerate into larger clusters, leading to the formation of BNNTs with larger diameters. Simultaneously, high temperature enhances the catalytic activity and the chemical reactions, resulting in more BN phase generation and thus more tube wall formation [36]. We suggest that after the quick crystallization of the thick BNNTs on the substrate surface, small catalyst particles condense on the surfaces of the tubes, leading to the formation of numerous narrow BNNTs in a flower-like structure, as depicted in figure 5(e). The growth mechanism for the secondary formation of these nanotubes is proposed to be a mixture of base-growth and tip-growth models for very thin BNNTs with diameters smaller than ~20 nm, and thin ones with diameters reaching ~40 nm, respectively. However, the latter ones were more frequently observed in TEM investigations.

### 3.3. Effect of metal oxide content

Early experiments on BNNTs in the past decade were carried out with different metal catalysts. Tang *et al* [33] reported

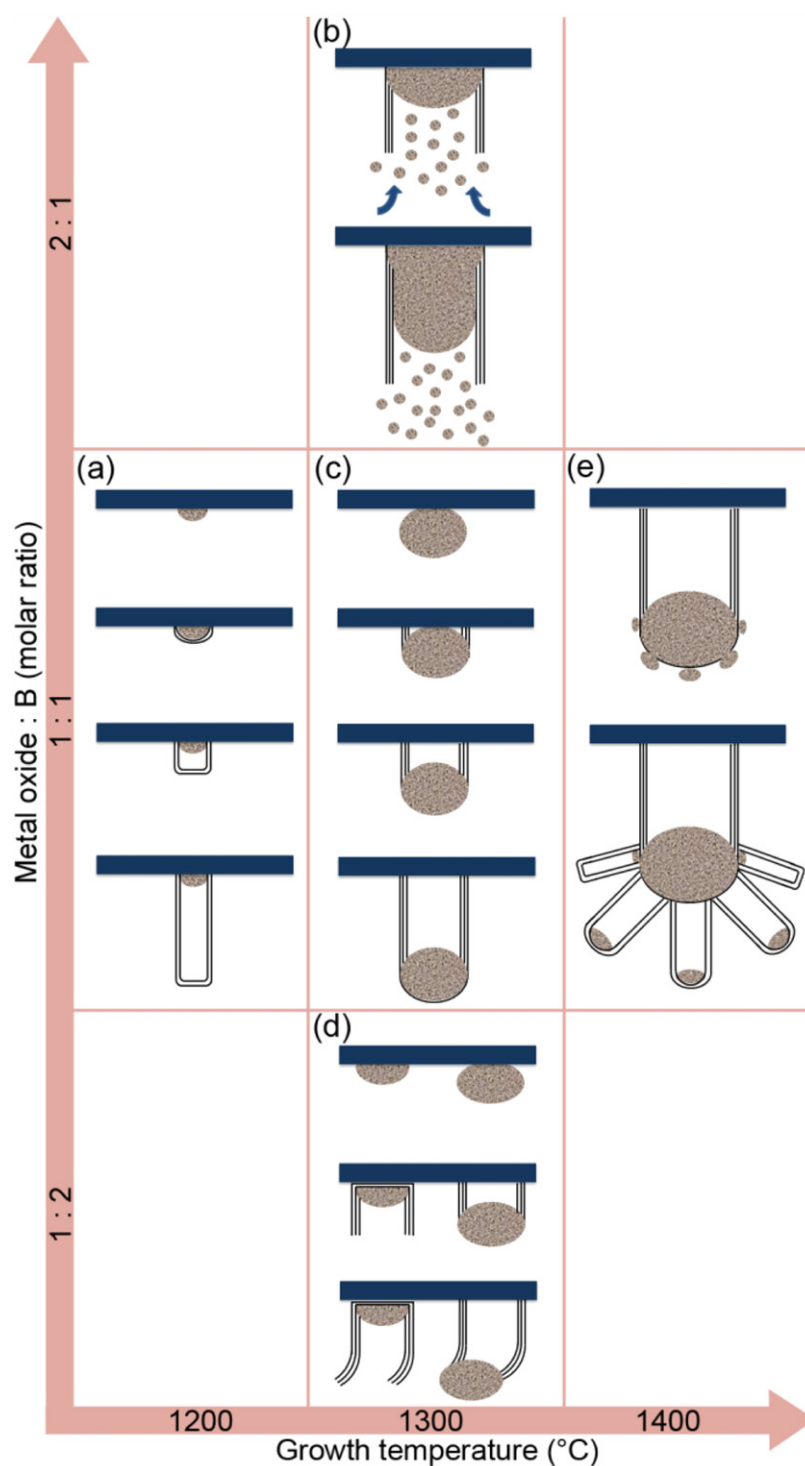


**Figure 5.** Suggested growth mechanisms for BNNTs synthesized in different conditions: (a) base-growth model, (b) tube filling during a base-growth model, (c) tip-growth model, (d) change of the growth direction in base-growth and tip-growth models, (e) mixed-growth model.

a carbon-free method for the synthesis of BNNTs through a chemical reaction of  $\text{NH}_3$  gas with  $\text{B}_2\text{O}_2$  generated from a mixture of MgO and B precursors. However, the growth of the BNNTs was slow due to the moderate catalytic activity of Mg [37]. As common catalysts for nanotube growth, different transition metals or their compounds have been tried for the synthesis of BNNTs, such as Ni, Co,  $\text{MoO}_3$ ,  $\text{V}_2\text{O}_5$ , CuO,

PbO, FeO,  $\text{Fe}_4\text{N}$  [5, 22, 38, 39]. However, the effectiveness of the chemical reaction of B and these materials has not been satisfying. Later, Zhi *et al* reported the mixture of FeO, MgO, and B powders to serve as a promising precursor for the synthesis of BNNTs due to the combination of the effective  $\text{B}_2\text{O}_2$ -producer and catalyst [37].

Besides the catalyst material, the catalyst content also plays an important role in the growth of nanotubes. To investigate the effect of catalyst concentration on the present BNNTs, the molar ratios of B:MgO:FeO were adopted as 1:1:1, 2:1:1, and 4:1:1. TEM investigations were performed on the 1D nanostructures synthesized at 1300 °C with different metal oxide contents. The low-magnification images of the products prepared with low metal oxide content displayed complex shapes for the as-grown curly BNNTs (supplementary data, figure S4 available at [stacks.iop.org/Nano/23/215601/mmedia](http://stacks.iop.org/Nano/23/215601/mmedia)). As illustrated in figures 3(d)(1) and (2), the curled tubes typically had closed tip-ends; however, tubes with open ends were also observed, as in figure 3(d)(3). Although the diameter was not usually very uniform over the entire length of the tubes, the average diameter of the curly BNNTs was measured as ~80 nm. HAADF STEM elemental mappings confirm the presence of Mg at the tip of the tubes, indicating catalytic growth of the curly BNNTs (supplementary data, figure S4, available at [stacks.iop.org/Nano/23/215601/mmedia](http://stacks.iop.org/Nano/23/215601/mmedia)). Here again, we suggest the VLS mechanism for the growth of the curly BNNTs; thus, the condensation of catalytic particles on the Si/SiO<sub>2</sub> substrate has been necessary to grow the nanotubes from their vapor species. The low content of metal oxides in the precursors, however, could result in a lesser distribution density of the catalytic particles on the substrate. Therefore, the BNNT bundles had more space to grow and thereby grew in a curly fashion. In addition, during the growth process, the BNNTs may bend if there are spatial fluctuations in the growth species precipitation causing nonuniform stresses at the particle/tube interface, as schematically depicted in figure 5(d). This mechanism has been discussed in detail for the growth of CNTs by Merkulov *et al* [40].

By increasing the metal oxide content, straight BNNTs with high aspect ratios were produced as illustrated earlier in figures 1(c), 2(c), and 3(b). Further increase in the metal oxides to B ratio (2:1) led to the growth of thick BN tubes and fibers with typical lengths of tens of micrometers (supplementary data, figure S5 available at [stacks.iop.org/Nano/23/215601/mmedia](http://stacks.iop.org/Nano/23/215601/mmedia)). A typical BNNT with a diameter of ~200 nm which encapsulates a particle at its tip is depicted in figure 4(b)(1). Figure 4(b)(2) represents a typical BN nanofiber (BNNF) with both open and closed tip-ends, having a nonuniform diameter of ~130 nm at the open tip and ~350 nm at the closed tip. The large diameters of the 1D BN products grown with higher metal oxide contents can be attributed to the cumulative catalytic nanoparticle density on the substrate and their sintering to form particles with large diameters. Another feature observed in plenty of the BNNTs synthesized with high metal oxide content was filling of the tubes, as illustrated in figures 4(b)(3) and (4) in the BNNTs with closed and open tip-ends, respectively. STEM-EDS analysis of the filled BNNTs suggests that the tubes are mainly filled with Mg (supplementary data, figure S5 available at [stacks.iop.org/Nano/23/215601/mmedia](http://stacks.iop.org/Nano/23/215601/mmedia)).

By comparing the TEM results of figure 4(b) and those of figures 4(a), (c), and (d), it can be concluded that the unfilled BNNTs with closed ends grew by the tip-growth

mechanism, while the filled ones grew in a different way. In the tip-growth model, the exposed end of the tube is filled with the catalyst particle and the opposite end is fixed to the substrate; therefore, it is unlikely that additional particles can gradually penetrate inside the tube. Hence, we suggest that the filled BNNTs initially grew by the base-growth mechanism, i.e., the catalyst particle remained fixed to the substrate and the tube grew open-ended. Therefore, there is the possibility for additional catalyst atoms to be accumulated along the length of the tube during the longitudinal growth, leading to lengthening of the initial catalyst particle inside the tube, as schematically depicted in figure 5(b). The capillary actions might have also contributed to the elongation of the catalyst material inside the tube. It has been reported that for tubes with large diameters, temporary lip–lip bonding between layers and the presence of metal catalyst particles can keep the tip-end open [41, 42]. As the open-ended BNNT grew, additional catalytic atoms could travel through this open channel, combine with the catalyst cluster and increase its initial size. However, considering the constraints from the walls of the tube, the additional growth had to be in the axial direction, resulting in a tube filled with the catalyst species [43]. The final length of the filled section would depend on the availability of additional catalyst species and the growth rate of the BNNT. If the BNNT grows very quickly compared to the elongation of the catalyst particle, the probability of metal atoms reaching the catalyst particle decreases due to the longer distance they have to travel through the tube [43]. Instead, the formation of new trapped particles is preferred, resulting in discontinuously filled BNNTs, as shown in figure 4(b)(5).

#### 4. Conclusion

A systematic study on the growth, morphology and structure of BNNT films synthesized by a catalytic CVD method was performed. The process variables (i.e., growth temperature and metal oxide content) immensely influenced the structural characteristics and growth mechanism of the BNNTs as follows: (a) raising the CVD growth temperature from 1200 °C increased the tubes' diameter, but the secondary growth of very thin tubes was observed at 1400 °C; (b) the BN nanotube films grown at 1200 and 1300 °C consisted of straight uniformly distributed tubes with high aspect ratios, while the ones grown at 1400 °C contained tube bundles with a flower-like structure; (c) we suggest that the nanotubes grown at 1200 °C and the very thin ones grown secondarily at 1400 °C grew by a base-growth mechanism, while the thick ones grown at 1300 and 1400 °C grew by a tip-growth mechanism; (d) the BN nanotubes synthesized with a low metal oxide content had a curly morphology, but the very thick ones synthesized with a high metal oxide content showed a randomly tilted semierect flower-like morphology; (e) the unfilled BN nanotubes grown via low/high metal oxide content with closed ends grew by a tip-growth mechanism, while the filled ones grew open-ended; thus additional catalyst atoms could accumulate at the open ends during growth, resulting in elongation of the existing particles and formation of filled tubes. The conclusion is summarized in table 1.

**Table 1.** The summary of the CVD growth of BNNT films.

B:MgO:FeO (molar ratio)	Temperature (°C)		
	1200	1300	1400
1:1:1		Diameter ~100–500 nm Semierect flower-like bundles Closed/open tip-ends Encapsulated Mg particles Unfilled/filled tubes Tip-/base-growth	
2:1:1	Diameter ~30 nm Straight randomly oriented Closed tip-ends No encapsulated particles Unfilled tubes Base-growth	Diameter ~60 nm Straight randomly-oriented Closed tip-ends Encapsulated Mg particles Unfilled tubes Tip-growth	Diameter ~ 20 and 100 nm Straight flower-like bundles Closed tip-ends Encapsulated Mg particles Unfilled tubes Mixed-growth
4:1:1		Diameter ~50–150 nm Entangled curly tubes Closed/open tip-ends Encapsulated Mg particles Unfilled tubes Tip-/base-growth	

## Acknowledgments

This work was supported by the National Institute for Materials Science (NIMS; Tsukuba, Japan) and was performed at the World Premier International Center for Materials Nanoarchitectonics (MANA; NIMS, Tsukuba, Japan). AP is grateful to Drs Jianxun Xu and Xuebin Wang for fruitful discussions, and Dr Yoshihiro Nemoto for assistance with the HRTEM. AP would like to thank Drs Kiyotaka Iiyama, Taketoshi Fujita, and Yoichiro Uemura for their technical support. DG also acknowledges the World Leading Scientists Grant Program (agreement No. 11.G34.31.0061) tenable at the National University of Science and Technology (MISIS; Moscow, Russia).

## References

- [1] Golberg D, Bando Y, Tang C C and Zhi C Y 2007 *Adv. Mater.* **19** 2413
- [2] Zhi C Y, Bando Y, Tang C C and Golberg D 2010 *Mater. Sci. Eng. R* **70** 92
- [3] Golberg D, Bando Y, Kurashima K and Sato T 2001 *Scr. Mater.* **44** 1561
- [4] Chen Y, Zou J, Campbell S J and Le Caer G 2004 *Appl. Phys. Lett.* **84** 2430
- [5] Golberg D, Bando Y, Huang Y, Terao T, Mitome M, Tang C C and Zhi C Y 2010 *ACS Nano* **4** 2979
- [6] Samanta S K, Gomathi A, Bhattacharya S and Rao C N R 2010 *Langmuir* **26** 12230
- [7] Chopra N G, Luyken R J, Cherrey K, Crespi V H, Cohen M L, Louie S G and Zettl A 1995 *Science* **269** 966
- [8] Golberg D, Bando Y, Eremets M, Takemura K, Kurashima K and Yusa H 1996 *Appl. Phys. Lett.* **69** 2045
- [9] Lourie O R, Jones C R, Bartlett B M, Gibbons P C, Ruoff R S and Buhro W E 2000 *Chem. Mater.* **12** 1808
- [10] Chen Y, Chadderton L T, FitzGerald J and Williams J S 1999 *Appl. Phys. Lett.* **74** 2960
- [11] Han W Q, Bando Y, Kurashima K and Sato T 1998 *Appl. Phys. Lett.* **73** 3085
- [12] Deepak F L, Vinod C P, Mukhopadhyay K, Govindaraj A and Rao C N R 2002 *Chem. Phys. Lett.* **353** 345
- [13] Bengu E and Marks L D 2001 Single-walled BN nanostructures *Phys. Rev. Lett.* **86** 2385
- [14] Shimizu Y, Moriyoshi Y, Tanaka H and Komatsu S 1999 *Appl. Phys. Lett.* **75** 929
- [15] Tang D M, Liu C and Cheng H M 2007 *J. Mater. Res.* **22** 2809
- [16] Oku T, Koi N, Narita I, Sugauma K and Nishijima M 2007 *Mater. Trans.* **48** 722
- [17] Lee C H, Wang J S, Kayatsha V K, Huang J Y and Yap Y K 2008 *Nanotechnology* **19** 455605
- [18] Pakdel A, Zhi C Y, Bando Y, Nakayama T and Golberg D 2011 *ACS Nano* **5** 6507
- [19] Huang Y, Bando Y, Tang C, Zhi C, Terao T, Dierre B, Sekiguchi T and Golberg D 2009 *Nanotechnology* **20** 085705
- [20] Celik-Aktas A, Zuo J M, Stubbins J F, Tang C and Bando Y 2005 *Appl. Phys. Lett.* **86** 133110
- [21] Saito Y, Maida M and Matsumoto T 1999 *Japan. J. Appl. Phys. I* **38** 159
- [22] Golberg D, Bando Y, Kurashima K and Sato T 2000 *Solid State Commun.* **116** 1
- [23] Oku T and Narita I 2004 *Diamond Relat. Mater.* **13** 1254
- [24] Huang Y, Lin J, Tang C C, Bando Y, Zhi C Y, Zhai T Y, Dierre B, Sekiguchi T and Golberg D 2011 *Nanotechnology* **22** 145602
- [25] Zhi C Y, Bando Y, Tang C C, Golberg D, Xie R G and Sekiguchi T 2005 *Appl. Phys. Lett.* **86** 213110
- [26] Yu J, Qin L, Hao Y F, Kuang S, Bai X D, Chong Y M, Zhang W J and Wang E 2010 *ACS Nano* **4** 414
- [27] Saha S, Muthu D V S, Golberg D, Tang C, Zhi C, Bando Y and Sood A K 2006 *Chem. Phys. Lett.* **421** 86
- [28] Arenal R, Ferrari A C, Reich S, Wirtz L, Mevellec J Y, Lefrant S, Rubio A and Loiseau A 2006 *Nano Lett.* **6** 1812
- [29] Gorbachev R V, Riaz I, Nair R R, Jalil R, Britnell L, Belle B D, Hill E W, Novoselov K S, Watanabe K, Taniguchi T, Geim A K and Blake P 2011 *Small* **7** 465
- [30] Loiseau A, Willaime F, Demoncey N, Hug G and Pascard H 1996 *Phys. Rev. Lett.* **76** 4737
- [31] Terrones M, Hsu W K, Terrones H, Zhang J P, Ramos S, Hare J P, Castillo R, Prassides K, Cheetham A K,

- Kroto H W and Walton D R M 1996 *Chem. Phys. Lett.* **259** 568
- [32] Iijima S, Ichihashi T and Ando Y 1992 *Nature* **356** 776
- [33] Tang C, Bando Y, Sato T and Kurashima K 2002 *Chem. Commun.* **12** 1290
- [34] Wagner R S and Ellis W C 1964 *Appl. Phys. Lett.* **4** 89
- [35] Meyyappan M, Delzeit L, Cassell A and Hash D 2003 *Plasma Sources Sci. T* **12** 205
- [36] Sinnott S B, Andrews R, Qian D, Rao A M, Mao Z, Dickey E C and Derbyshire F 1999 *Chem. Phys. Lett.* **315** 25
- [37] Zhi C Y, Bando Y, Tan C C and Golberg D 2005 *Solid State Commun.* **135** 67
- [38] Ma R Z, Goldberg D, Bando Y and Sasaki T 2004 *Phil. Trans. R. Soc. A* **362** 2161
- [39] Oku T, Koi N, Suganuma K, Belosludov R V and Kawazoe Y 2007 *Solid State Commun.* **143** 331
- [40] Merkulov V I, Melechko A V, Guillorn M A, Lowndes D H and Simpson M L 2001 *Appl. Phys. Lett.* **79** 2970
- [41] Kwon Y K, Lee Y H, Kim S G and Jund P 1997 *Phys. Rev. Lett.* **79** 2065
- [42] Bernholc J, Brabec C, Nardelli M B, Maiti A, Roland C and Yakobson B I 1998 *Appl. Phys. A* **67** 39
- [43] Deck C P and Vecchio K 2005 *Carbon* **43** 2608